High-Resolution Force Control in a Multi-Pressure Hydraulic System for Excavator Work Functions

Mohamed Allam[1], Mikko Huova[1], Kim Heybroek[2]

[1]Tampere University, Tampere, Finland, mohamed.allam@tuni.fi, mikko.huova@tuni.fi

[2]Volvo Construction Equipment, Eskilstuna, Sweden, kim.heybroek@volvo.com

Abstract

Conventional centralized throttling-based hydraulic systems in excavators are robust but inefficient, especially under partial loads and multi-actuator operation. To address the inefficiencies, this work presents a multi-pressure hydraulic system for a 20-ton excavator and the implementation of its control. The system employs four discrete pressure levels, maintained by accumulators and a displacement-controlled pump, and distributed to the Swing, Boom, Arm, and Bucket actuators via 2/2 proportional valves. This enables more efficient use of energy but requires the development of a controller to select the pressure level, meter the flow and maintain machine performance. A force-based control strategy is developed that can manage these tasks while remaining relatively simple for practical implementation. The proposed controller combines discrete pressure levels with continuous modulation yielding near-continuous force resolution. Simulation in MATLAB/Simulink demonstrates 67% reduction in energy consumption against the original machine's load sensing system, and a 32% reduction against a benchmark controller developed previously for the multi-pressure system. Results also showed accurate tracking and preserved actuator dynamics.

Keywords: Mobile Machines, Hybrid Systems, Multi-Pressure System, Excavators, Control, Energy Efficiency, Force Control, Novel System.

1. Introduction

Hydraulic systems are extensively employed in heavy machinery due to their high-power density and robust performance. However, traditional hydraulic architectures, particularly those relying on throttling-based flow control, often exhibit energy losses. These conventional systems lack regeneration capabilities, differential flow control, and independent metering, resulting in inefficiencies. Recent research has focused on enhancing the energy efficiency of hydraulic work functions through various methods, including hydraulic transformers [1], multi-chamber cylinders [2], displacement control [3], hybrid technologies [4], and electro-hydraulic actuators [5]. Despite demonstrating significant energy savings, none of these approaches has yet seen widespread industrial adoption. While these solutions hold promise for future mobile machinery applications, this study pursues a multi-pressure system (MPS) approach. In an MPS, the actuator is connected to a discrete number of pressure levels achieving several different control modes that can be increased tremendously when coupled with proportional valves which requires the development of an appropriate control algorithm. The controller needs to accomplish different tasks simultaneously such as selection of pressure levels, modulation of proportional valves and management of mode switching.

Several authors have addressed the challenge of discrete multi-pressure or multi-chamber system control. For instance, Heybroek [6] applied model predictive control to balance force peaks and energy efficiency. Hansen proposed a force switching algorithm for wave energy converters [7]. Huova also presented controllers for a multi-pressure actuator [8] and also tackled a model predictive control for a MPS in [9]. Xu also presents an actuator controller for a Multi-pressure multi-chamber cylinder system, which handles the pressure trajectories during transients using a MPC [10]. Building upon the insights presented in these research, the force-based controller developed in this work integrates concepts from Linjama's [2] work on secondary control along Hansen's [11] effort in reducing pressure oscillations to yield a practical and implementable control solution for the MPS.

This paper presents the development and evaluation of a force-based control strategy aimed at maximizing the energy-saving potential of the MPS. The proposed controller uses velocity feedback to generate a reference force needed to accelerate the piston and dynamically selects the chamber pressure levels maintaining controllability and reducing losses. The algorithm generates valve commands for both inflow and outflow actuator valves to satisfy operator inputs. This control approach also effectively mitigates force peaks caused by the different pressure dynamics during a mode switch in individual actuator chambers, as detailed in the control algorithm section. The proposed controller is benchmarked against a previously developed concept and the original machine's system using simulations.

2. System Architecture

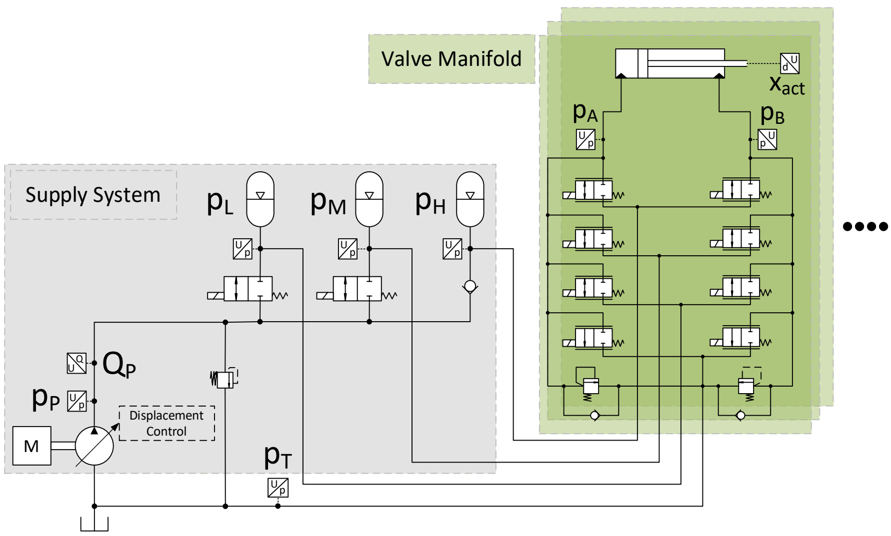

Figure 2.1: Simplified hydraulic circuit diagram of the Multi-Pressure System detailing the supply system and valve manifolds

The MPS illustrated in Figure 2.1. consists of three hydraulic accumulators operating at different pressure levels $[p_L, p_M, p_H]$ and a tank line p_T which establishes the system's multi-pressure supply lines. These lines are connected to the excavator's hydraulic work functions

[Swing, Boom, Arm, Bucket] via valve manifolds equipped with sets of 2/2 proportional bidirectional valves. Each valve modulates flow into and out of the actuator chambers by connecting to the appropriate pressure line and controlling flow metering in both piston and rod chambers. Pressure sensors on both actuator ports and a piston position sensor deliver feedback signals essential to the valve controller functionality. This feedback enables the control of valve commands to achieve desired actuator force outputs. The accumulator pressure levels are maintained between set thresholds by the excavator's hydraulic supply system, comprising of a diesel engine coupled to a variable-displacement piston pump. The pump output is regulated to charge the accumulators through dedicated charge valves.

3. Control Algorithm

In the proposed MPS each actuator manifold contains four proportional bi-directional valves at the piston side and four at the rod side each connected to a pressure level. The role of the control algorithm is to choose the appropriate pressure level and actuate its corresponding valve according to the system requirements and load conditions. This is accomplished by using signals from the chamber $[p_A, p_B]$ and supply line pressures $[p_T, p_L, p_M, p_H]$, the cylinder position x as well as the joystick signal from the operator v_{ref} and the piston velocity v which can be estimated from the position sensor. The next section presents how the controller is formulated and how each decision is made, and the overall flow of the algorithm is shown in Figure 3.1.

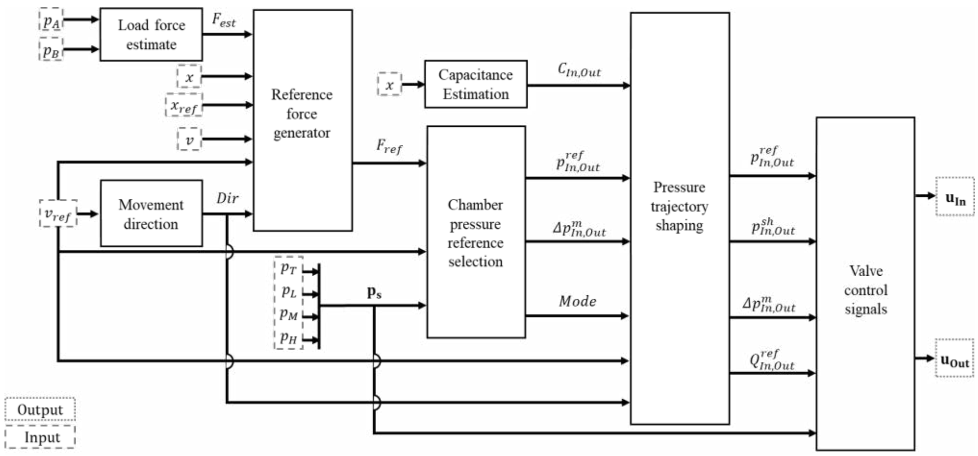

Figure 3.1: Force control algorithm - overall flow

The main idea is to generate a reference force F_{ref} based on the velocity error between the velocity reference v_{ref} (which could be e.g. a joystick command) and the measured velocity estimated from the piston position x (in case of a cylinder actuator). Following the force reference requires high resolution of achievable forces which can be accomplished by on/off-type control of the valves, for example, as demonstrated in Linjama [2]. However, when using two-chamber cylinders and four discrete pressure levels, the resolution obtained in this way is not sufficient for practical operation. To overcome this limitation, the proportional control valves employed are used to introduce a pressure differential in each of the chambers, thereby enabling finer adjustment of the actuator forces and significantly improving the achievable force resolution.

The pressure selection chooses chamber pressure references for the inflow and outflow sides $p_{In,Out}^{ref}$ that match the generated reference force. The chamber reference selection is done through a cost function that minimizes force error, unnecessary variation of chamber pressures and power losses.

In the next step, the valve commands are selected such that the chamber pressure references are achieved. The references are generated in two different ways depending on the operating condition. During regular motion, when no pressure transient is needed i.e., during a pressure shift, it is kept as the selected pressure reference, whereas during a pressure shift where the selected lines are changed, it follows a predefined pressure trajectory $p_{In,Out}^{Sh}$. In both cases, the valve commands are determined based on the required flow rate and the calculated pressure differential, which accounts for both the supply pressure and the chamber pressure reference. The required flow rate is obtained from the piston velocity, the derivative of the chamber pressure reference, and the estimated hydraulic capacitance. This is done in order to avoid force peaks originating from different pressure dynamics in the piston and rod side chambers during a mode switch. The details of each step are illustrated in the next sections.

3.1. Movement direction

The first step is determining the movement direction of the actuator's piston. This is done using the velocity reference generated by the operator. This step is necessary to assign the variables of the controller to the inflow and outflow sides. Where the variable Dir is calculated using:

$$Dir = \begin{cases} 1 \quad If \begin{cases} v_{ref} \geq v_{start}\, OR \\ v_{ref} > v_{stop}\, AND\, Dir^{-1} = 1 \end{cases} \\ -1 \quad If \begin{cases} v_{ref} \leq -v_{start}\, OR \\ v_{ref} < -v_{stop}\, AND\, Dir^{-1} = 1 \end{cases} \\ 0 \quad else \end{cases} \tag{1}$$

The logic includes hysteresis to avoid repetitive initiation of motion, where v_{start} and v_{stop} are velocity thresholds to start and stop the movement and Dir^{-1} is the direction variable in the previous timestep. The parameters, inputs and outputs of the control algorithm are assigned based on the value of the direction variable to the inflow and outflow sides. The logic is used throughout the controller, and an example is shown for the effective areas of the chambers for the inflow A_{In} and the outflow A_{Out} where:

$$A_{In} = \begin{cases} A_A & Dir \geq 0 \\ A_B & Dir < 0 \end{cases} ; A_{Out} = \begin{cases} A_B & Dir \geq 0 \\ A_A & Dir < 0 \end{cases} \tag{2}$$

where A_A and A_B are the chambers effective areas on the piston and rod sides.

3.2. Reference force generator

The reference force is generated using a PI – controller based on the velocity error. An outer position loop is added to the existing velocity controller to correct for position error where the corrected reference velocity v_{ref_x} is calculated using:

$$v_{ref_x} = \left(x_{ref}(t) - x(t)\right)K_{px} + v_{ref} \tag{3}$$

where x_{ref} is the position reference, K_{px} is the gain for position loop. The reference force F_{ref} is generated using:

$$F_{ref} = \left(v_{ref_x} - v\right)K_P + K_I \int \left(v_{ref_x} - v\right)dt \tag{4}$$

K_p and K_i are the proportional and integral gains respectively and v is the measured piston velocity. An important note, in operating intervals where no velocity command is provided by the operator, i.e. *Dir* equals zero, the reference force is gradually driven toward an estimated hydraulic force F_{est}, computed from the measured chamber pressures as:

$$F_{est} = p_A A_A - p_B A_B \tag{5}$$

The motivation for this is to prevent delays or wrong movement directions when valve actuation starts. By aligning the reference force with the estimated force during inactive periods, the system ensures a smooth transition between inactive and active phases of operation, thereby improving responsiveness and allowing for smoother operation.

3.3. Chamber pressures selection

The principle of pressure selection is to match the reference force by choosing appropriate chamber pressures from a set of virtual levels. Since there is a limited number of accumulators and they cannot provide arbitrary pressure values, intermediate pressure levels are virtually generated by linearly interpolating between the current accumulator pressures. These "virtual" levels represent pressures that can be realized in practice through throttling across the metering valves for the inflow and outflow sides. The available accumulator pressures $\mathbf{p_s}$, is defined as:

$$\mathbf{p_s} = [p_T, p_L, p_M, p_H] \tag{6}$$

These serve as the boundary values for constructing virtual multi-level buses along with the minimum and maximum system pressures. This produces a denser grid of chamber pressures for the inflow and outflow sides using the constructed vector $\mathbf{p_{virt}}$. The vector expands the resolution of the achievable force levels beyond the discrete accumulator values while preserving physical feasibility. A combination matrix $\mathbf{M}$ is formed based on the number of virtual levels n created where:

$$\mathbf{M} = \begin{bmatrix} 1 & 1 & \dots & 1 & 2 & 2 & \cdots & n \\ 1 & 2 & \dots & n & 1 & 2 & \cdots & n \end{bmatrix} \tag{7}$$

where the matrix $\mathbf{M}$ has the size $2\mathrm{x}n^2$. Pressure references are created using the vectors $\mathbf{p_{In}^{ref}}$, $\mathbf{p_{Out}^{ref}}$ and $\mathbf{p_{virt}}$:

$$\begin{aligned} \mathbf{p_{In}^{ref}} &= \mathbf{p_{virt}}\left(\mathbf{M}(1,:)\right) \\ \mathbf{p_{Out}^{ref}} &= \mathbf{p_{virt}}\left(\mathbf{M}(2,:)\right) \end{aligned} \tag{8}$$

For each candidate pair of inflow and outflow side pressures an achievable actuator force **F** is calculated where:

$$\mathbf{F} = \mathbf{p}_{\mathbf{In}}^{\mathbf{ref}} \mathrm{A}_{\mathrm{in}} - \mathbf{p}_{\mathbf{Out}}^{\mathbf{ref}} \mathrm{A}_{\mathrm{Out}} \tag{9}$$

where A_{in} and A_{Out} are the effective areas of the inflow and outflow sides dictated by the Dir variable.

To calculate the static power losses for the cost function each candidate is paired with an accumulator that can meter the flow in or out of the chamber depending on the direction of motion. For the inflow side an accumulator with higher or equal pressure to the virtual chamber pressure reference is chosen and for the outflow side an accumulator with lower or equal pressure is chosen. This creates the bus matrices $\mathbf{p}_{\mathbf{In}}^{\mathbf{Bus}}, \mathbf{p}_{\mathbf{Out}}^{\mathbf{Bus}}$. The two vectors can be used to calculate the throttle free force and consequently the static power loss $\mathbf{P}_{\mathbf{loss}}$ where:

$$\mathbf{P}_{\mathbf{loss}} = \left(\left(\mathbf{p}_{\mathbf{In}}^{\mathbf{Bus}} A_{In} - \mathbf{p}_{\mathbf{Out}}^{\mathbf{Bus}} A_{Out}\right) - \mathbf{F}\right) * |v_{ref}| \tag{10}$$

On the other hand, not all chamber pressures are hydraulically realizable. Therefore, a feasibility check is performed to eliminate the unfeasible pairs where:

$$\begin{aligned} \mathbf{feas} = \mathbf{p}_{\mathbf{In}}^{\mathbf{Bus}} - \mathbf{p}_{\mathbf{In}}^{\mathbf{ref}} &\geq \Delta p_{In}^{m} \text{ AND} \\ \mathbf{p}_{\mathbf{In}}^{\mathbf{Bus}} &> 0 \text{ AND} \\ \mathbf{p}_{\mathbf{Out}}^{\mathbf{ref}} - \mathbf{p}_{\mathbf{Out}}^{\mathbf{Bus}} &\geq \Delta p_{Out}^{m} \end{aligned} \tag{11}$$

Where Δp_{In}^{m} and Δp_{Out}^{m} are the minimum differential pressure across the valve to allow for metering and is calculated using the valve orifice equation:

$$\Delta p_{In,Out}^{m} = \left(\frac{A_{In,Out} v_{ref}}{K_{In,Out}^{V}}\right)^2 \tag{12}$$

where $K_{In,Out}^{V}$ is the valves flow coefficient calculated using the nominal flow rate and pressure difference.

A cost function **J** is formulated to choose the reference chamber pressures for the inflow and outflow where:

$$\begin{aligned} \mathbf{J} = \left|\mathbf{F} - F_{ref}\right| + W_{prs}\left(\left|p_{In}^{ref^-} - \mathbf{p}_{\mathbf{In}}^{\mathbf{ref}}\right| A_{In} - \left|p_{Out}^{ref^-} - \mathbf{p}_{\mathbf{Out}}^{\mathbf{ref}}\right| A_{Out}\right) \\ + W_{loss} \mathbf{P}_{\mathbf{loss}} + W_{dp} \boldsymbol{\Delta} \mathbf{p}_{\mathbf{eq}} \end{aligned} \tag{13}$$

where W_{prs}, W_{loss} and W_{dp} are weighing terms for the static losses, the magnitude of the chamber pressure change and for equalizing the pressure differential at the inflow and outflow sides, $p_{In}^{ref^-}$ and $p_{Out}^{ref^-}$ are the selected chamber pressure references at the previous time step.

The final term in the cost function attempts to ***equally*** distribute the needed overall pressure differential to both the inflow and outflow sides, this helps in reducing the valve activity and also avoids having high pressure difference in the inflow side and low-pressure difference on the outflow side. The term $\boldsymbol{\Delta}\mathbf{p}_{\mathbf{eq}}$ is calculated using:

$$\boldsymbol{\Delta}\mathbf{p}_{\mathbf{eq}} = \left|\left(\mathbf{p}_{\mathbf{In}}^{\mathbf{Bus}} - \mathbf{p}_{\mathbf{In}}^{\mathbf{ref}}\right) - \left(\mathbf{p}_{\mathbf{Out}}^{\mathbf{ref}} - \mathbf{p}_{\mathbf{Out}}^{\mathbf{Bus}}\right)\right| \tag{14}$$

The infeasible combinations are set to infinity and the chosen chamber pressure references for the inflow p_{In}^{ref} and outflow p_{In}^{Out} sides are chosen as:

$$p_{In,Out}^{ref} = \mathbf{p}_{\mathbf{In,Out}}^{\mathbf{ref}}[k] \tag{15}$$

where k is the index of minimizing the cost function. Each selected chamber pressure has a corresponding chosen accumulator that is combined to the $Mode$ variable where:

$$Mode = \left[\mathbf{p}_{\mathbf{In}}^{\mathbf{Bus}}(k)\ \mathbf{p}_{\mathbf{O}ut}^{\mathbf{Bus}}(k)\right] \tag{16}$$

The chosen chamber pressure references $\left[p_{In}^{ref}, p_{Out}^{ref}\right]$, and M$ode$ are input to the trajectory shaping algorithm which is explained in the next section.

3.4. Pressure trajectory shaping

Chamber pressure references can change in two ways, which determines how valve commands are generated. For small changes within the chamber that do not require switching accumulators; flow is displacement induced, and valve commands are computed using the calculated pressure differential (supply and chamber reference) and the valve orifice equation. Larger changes, which require one or both chambers to switch accumulators, actuate multiple valves simultaneously can produce a “force peak”. Uneven pressure build-up owed to different hydraulic capacitance results in sudden acceleration or deceleration of the piston due to the force peak. To prevent this, valve commands are shaped to make the chamber pressures follow a predefined pressure trajectory. The implemented algorithm is derived from the work in [11].

The idea is to generate a flow rate reference Q_{ref} and consequently a valve opening u_v that corresponds to the pre-defined pressure trajectory. The trajectory used in this work is a third order polynomial which is calculated from:

$$p_{In,Out}^{sh} = -\frac{2\Delta p_{In,Out}}{\tau_{Sw}^3} t^3 + \frac{3\Delta \mathrm{p}_{In,Out}}{\tau_{Sw}^2} t^2 + p_{In,Out}^0 \tag{17}$$

where $\Delta p_{In,Out}$ can be defined as:

$$\Delta p_{In,Out} = p_{In,Out}^{ref} - p_{In,Out}^0 \tag{18}$$

and p_0 is the chamber pressure at the beginning of the shift, t is the current time step and τ is the time dedicated for the pressure switch to be completed.

To calculate the flow rate reference needed to complete the pressure switch for both sides, the pressure build-up equation can be used after re-arranging for Q_{In}^{ref} where:

$$\begin{aligned} Q_{In}^{ref} &= A_{In} v_{ref} + C_{In}\left(-\frac{6\Delta p_{In}}{\tau_{Sw}^3} t^2 + \frac{6\Delta p_{In}}{\tau_{Sw}^3} t\right) \\ Q_{Out}^{ref} &= -A_{Out} v_{ref} + C_{Out}\left(-\frac{6\Delta p_{Out}}{\tau_{Sw}^3} t^2 + \frac{6\Delta p_{Out}}{\tau_{Sw}^3} t\right) \end{aligned} \tag{19}$$

where C_{In} and C_{Out} are the hydraulic capacitances estimated from the piston position [12].

It is important to note that the pressure shaping algorithm is only active at times where there is a mode switch occurring dictated by the variable $Mode$ changing values. When no mode switching is occurring the valve commands are calculated using the displacement flow reference which is the first part of equation (19) and $p_{In,Out}^{sh}$ are set as $p_{In,Out}^{ref}$.

3.5. Valve actuation logic

The valve reference generation for the inflow and outflow sides is formulated such that the reference flow rates $Q_{In}^{ref}, Q_{Out}^{ref}$ are distributed to the accumulators that are hydraulically feasible. For the inflow side, the accumulator is considered feasible If the pressure differential to p_{In}^{sh} is higher than or equal to Δp_{In}^{m}. The feasible accumulators are sorted by their proximity to p_{In}^{ref} at each time step. The maximum achievable flow from one accumulator is calculated from:

$$Q_{In,Out}^{max} = \begin{cases} K_{In}^{V}\sqrt{\mathbf{p_s}(j) - p_{In}^{sh}} & \mathbf{p_s}(j) - p_{In}^{sh} \geq \Delta p_{In}^{m} \\ -K_{Out}^{V}\sqrt{p_{Out}^{sh} - \mathbf{p_s}(j)} & p_{Out}^{sh} - \mathbf{p_s}(j) \geq \Delta p_{Out}^{m} \end{cases}$$

where j is the index of the feasible accumulator after sorting. The valve command is then calculated using:

$$u_{In,Out}(j) = \frac{Q_{In,Out}^{ref}}{Q_{In,Out}^{max}} \tag{20}$$

and the non-feasible indices are set to zero. If the valve is not fully opened this means that the flow reference is satisfied. However, if the opening is more than one this means that another valve needs to be opened to meet the requirement. This is done by setting the current valve to fully open and the new flow reference to the difference between current valve's maximum flow and the original flow required and calculating the opening using the new reference. The outflow side is calculated in a similar fashion with the main difference being that the p_{Out}^{sh} must be higher than accumulator pressure by Δp_{Out}^{m}. Finally, the inflow and outflow valve commands $\mathbf{u_{In}}$, $\mathbf{u_{Out}}$ are routed to the piston and rods sides using the Dir variable.

4. SIMULATION AND RESULTS

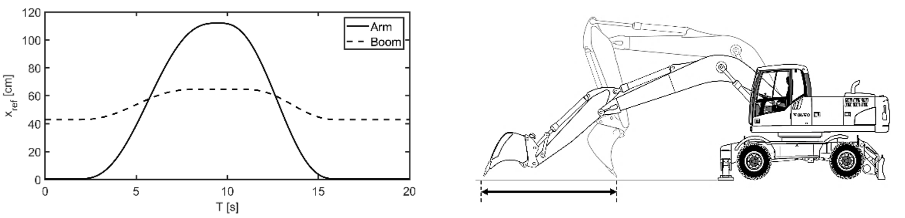

(a) (b)

Figure 4.1: (a) Reference trajectories for the boom and arm actuators (b) Motion of the machine's components relative to the commands

The simulation uses a 20s air grading cycle from the JCMAS standard which is shown in Figure 4.1, where the boom and arm cylinders are extended and retracted simultaneously representing a leveling operation. The cycle was adopted for this simulation study as it is well established in literature and provides a suitable basis for evaluating system performance under multi-actuator operation and high flow demands [13]. It is also based on measurements performed with the original base-line machine performing the same trajectories. The detailed simulation model, cycle description and the previously developed controller, used here as a benchmark, are presented in [14]. In this work, the focus is on assessing the proposed force-based controller relative to that benchmark as well as the original machine's system which is also detailed in the cited publication. The main parameters used in the simulation model are listed in Table 4.1 while the controller parameters are illustrated in Table 4.2.

Table 4.1: Main parameters for the simulation

Machine mass	21160	kg
Accumulator pressure	[0, 106, 213, 320]	bar
Valve coefficient K_V	$1.088\text{x}10^{-5}$	$\mathrm{m^3/(s.Pa^{1/2})}$
Valve delay	30	ms
Valve time constant	10	ms

Table 4.2: Control algorithm parameters

K_P	$[2\text{x}10^5, 1\text{x}10^6]$ *	N/(m/sec)
K_I	$2.5\text{x}10^6$	1/sec
K_{px}	2	1/sec
v_{start}	$2\text{x}10^{-3}$	m/sec
v_{stop}	$1\text{x}10^{-3}$	m/sec
n	49	ul
W_{loss}	[0.65, 4]*	W
W_{prs}	[0.01, 0.02]*	ul
W_{dp}	$2.5\text{x}10^{-3}$	Pa
τ_{Sw}	90	ms

****Arm, Boom***

4.1. Performance

Figure 4.2 and Figure 4.3 show the simulation results for the boom and arm cylinders during the simulated cycle. The first two plots show the position and velocity tracking. The second diagram shows the multi-pressure lines, chamber pressure references, shaped chamber pressures and finally the simulated chamber pressures. Next diagram illustrates the forces including the reference force F_{ref}, selected force (representing the selected pressure references $p_{In,Out}^{ref}$), shaped force (representing the shaped pressure references $p_{In,Out}^{sh}$) and finally the boom force calculated from the chamber areas and pressures. Finally, the valve commands for the piston (A) and rod (B) sides are shown where the colors match those of the pressure lines in the third plot.

Figure 4.2 illustrates the dynamic behavior of the boom actuator, highlighting the performance of the control strategy and MPS. The piston velocity and position closely follow their reference trajectories, indicating that the controller tracks the commanded inputs well. Minor deviations in velocity tracking are observed during both extension and retraction phases attributable to arm motion conditions. However, these do not significantly affect the position tracking of the boom, which remains accurate throughout.

The tracking performance is enabled by the regulation of chamber pressure references to follow the reference force, as shown in the pressure subplot. At the start of motion, when the piston velocity is low, the controller connects piston side chamber to the medium-pressure line and the rod side chamber to the low-pressure line. This configuration allows the tracking of the desired reference force through throttling on both sides. As the piston velocity increases along with associated power losses the controller transitions piston side chamber to the low-pressure line and the rod side chamber to the tank-line. This mode is maintained throughout the extension phase as it balances between force tracking and static losses. As the piston approaches its target position and decelerates, the controller reduces the output force as needed by increasing the pressure in the rod side chamber while simultaneously decreasing the pressure in piston side chamber. This allows close tracking of the reference force that is decreasing.

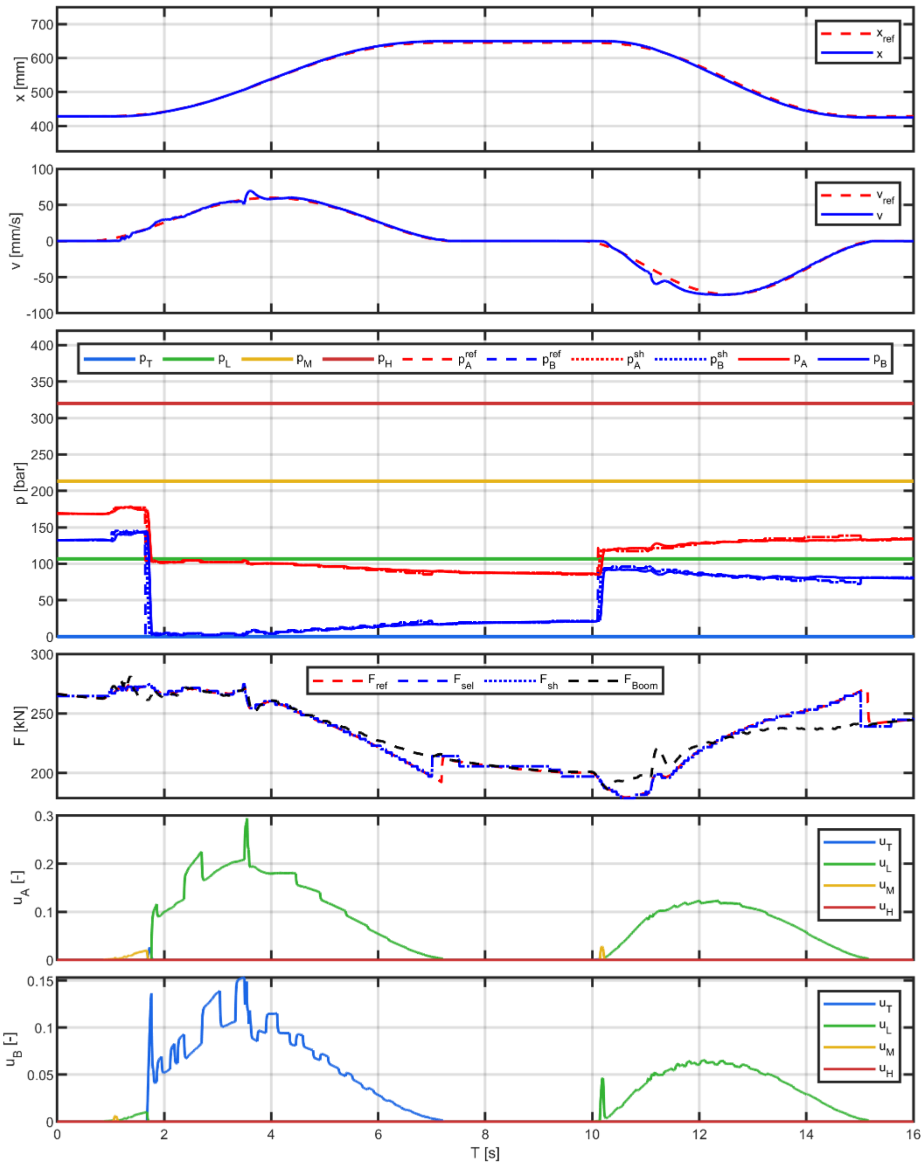

Figure 4.2: Simulation results for the control algorithm of the boom actuator

During retraction, both chambers are connected to the low-pressure line, implementing a differential flow strategy. When the reference force increases, the controller responds by raising the pressure in the piston side chamber and reducing the pressure in the rod side chamber, thereby maintaining effective velocity tracking while reducing the losses. There is an instance where the controller operates at near minimum pressure differential for both chambers at the start of retraction motion contributing to fewer losses and is a core strength of the proposed logic. Additionally, it can be seen that the chamber pressure references change in a stepwise manner at mode switches, but the actual pressures follow the trajectory shaping pressure reference which is detailed more in the upcoming sections.

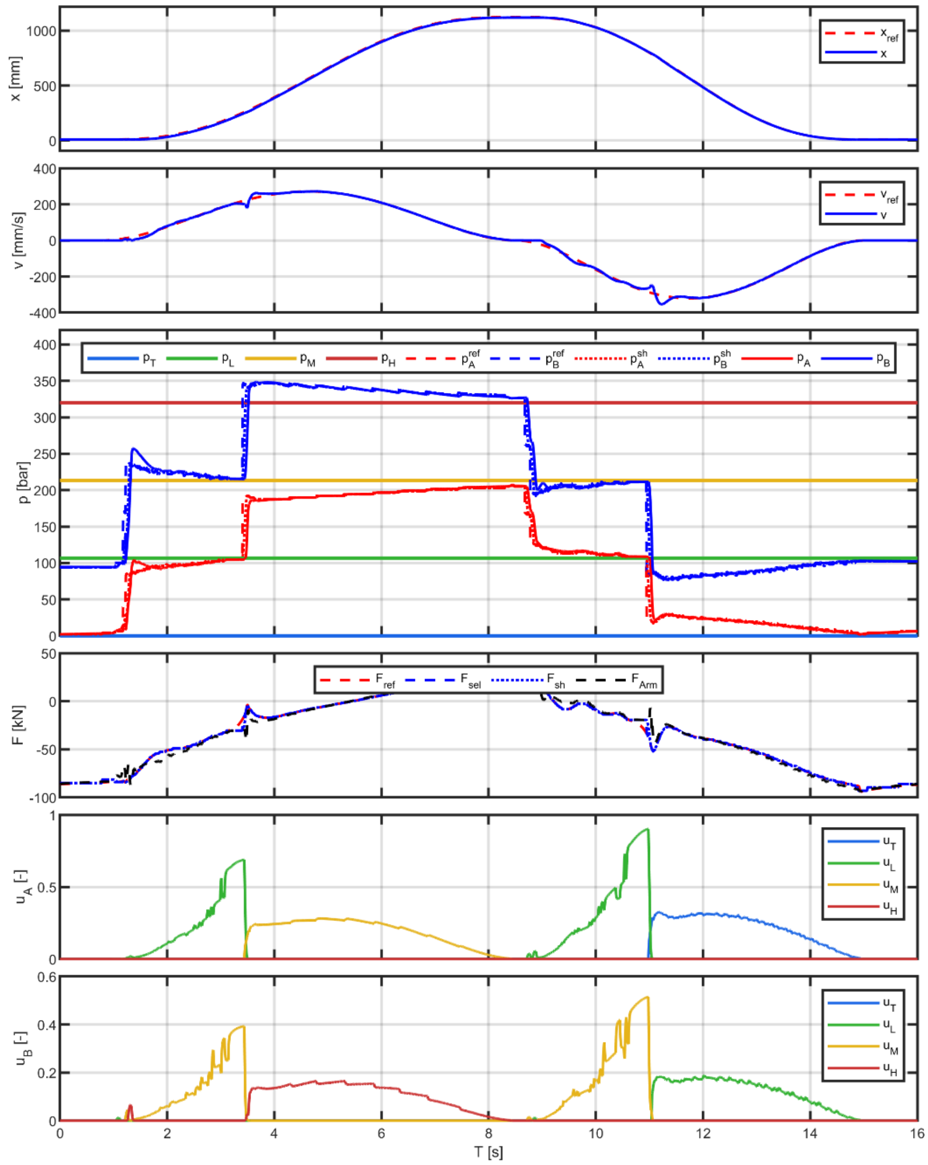

Figure 4.3: Simulation results for the control algorithm of the arm actuator

The arm actuator shows similar results in terms of precise velocity and position tracking with the similar observation of smaller deviations in velocity that are not noticed in position response during motion. The arm actuator chamber pressure references show more activity than the boom actuator mainly due to the force distribution resulting from the available pressure levels and effective areas.

At the beginning, the piston side chamber is connected to low-pressure line while the rod side chamber is connected to medium-pressure line achieving the required negative reference force. Similarly to the boom actuator, the reference force is matched by increasing the pressure in the piston side chamber and reducing pressure in the rod side chamber. The deviation in velocity seen at around 3.5 seconds is due to the algorithm selecting a mode with negative force error that enables reduction of power losses, which is another key strength of the proposed controller in terms of energy savings. As the force error increases the algorithm shifts to reduce the error and introduces throttling as a consequence where it now chooses medium-line for piston side and high-line for rod side. This mode is kept for the rest of the duration of extension. The reference force is again matched by manipulating the chamber pressure references for both edges.

During retraction, the controller initially selects low-line for the piston side chamber and high-line for the rod side chamber. As the losses increase quickly the chambers are switched to a lower pressure reference using the same line for the piston side chamber and switching to medium-line for the rod side chamber, which yields lower losses. The mode remains feasible and highly efficient as it has near minimum pressure differential. The force reference is again matched by regulating both chamber pressures until just before 11 seconds, where it becomes infeasible. At this instance, some force error is allowed by the controller to reduce losses before switching to a different mode which can be seen in the velocity tracking (piston slowing down then speeding back up). To reduce the force error, the control switches to a different mode that can match the reference at the cost of power losses. The chosen mode is tank for the piston side chamber and low for the rod side chamber. Similarly to the end of the extension stroke the mode is preserved and the force reference is matched by increasing the pressure in the rod side chamber and reducing the pressure in the piston side chamber.

The stepwise nature of some of the valve command signals on both sides of both actuators is attributed to the discrete pressure reference selection algorithm. While this approach simplifies implementation, it introduces a higher utilization of the valves. A finer and more consistent valve command profile could be achieved by increasing the number of virtual pressure levels available n. This would enhance control resolution, but at the cost of increased computational load. An optimization study for the number of virtual levels along with other parameters are left for future studies.

4.2. Pressure trajectory shaping

The pressure shaping algorithm is illustrated in Figure 4.4 where the top figures show the pressures in both chambers and how they evolve during the switching period $[t_0 \rightarrow \tau_{Sw}]$ and their corresponding flow rate references in the bottom plots.

The figure highlights the pressure shift occurring in the boom actuator just before 2 seconds during extension. For piston side chamber the pressure reference shifts from medium to low.

It can be seen that the pressure reference p_A^{ref} changes instantly while the chamber pressure steadily follows the generated shaped pressure reference shown in dotted. This is accomplished by modifying the flow rate reference using the third order polynomial defining the needed flow to complete the shift. Initially, the flow rate reference is due to the displacement flow needed by the piston motion, at the instant where the chamber reference shifts the flow reference is modified to shape the chamber pressure. The reference is followed by sequential valve control starting with closing the medium-line valve to reduce the flow rate and pressure as needed, then opening the tank valve to supply the required negative flow (flow out of the chamber) which reduces the pressure further. At the end of the shift the low line valve is opened to complete the shift and continue supplying the displacement flow.

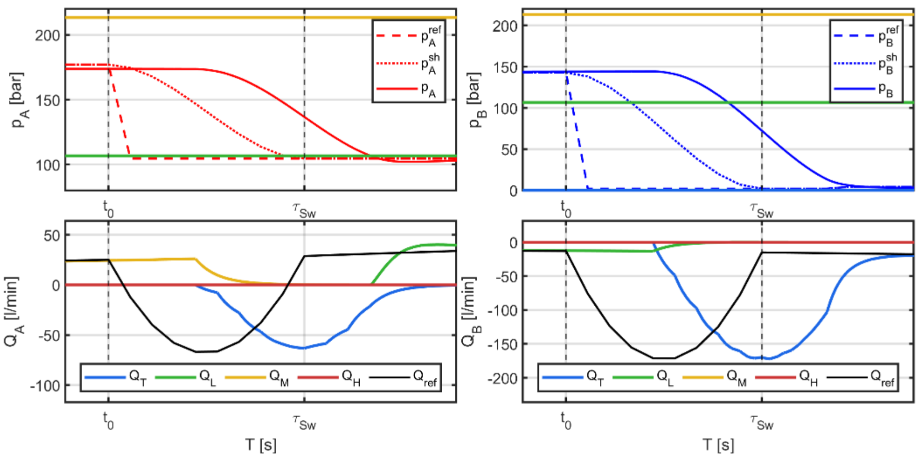

Figure 4.4: An excerpt from the results highlighting the pressure shaping algorithm

On the other hand, at the rod side chamber (figure to the right) similar behavior is observed with the exception that the flow reference doesn't change signs during the shift. The shaping can be accomplished by closing the low-pressure line valve and then opening the tank-line valve. More details on the reasoning behind flow direction changes can be found in Hansen's work [11]. The delay between the flow rate reference and the achieved one is attributable to the valve dynamics. Finally, it is important to note that the switching time τ_{Sw} is set to 90 ms and the sampling rate is 10 ms which explains the steps in the flow rate signal.

4.3. Energy savings

A key strength point of the proposed algorithm is that it enables metering of the flow with minimum required differential pressure accomplished by manipulating the chamber pressure references. This is reflected in the power consumption of both actuators where there are several instances of the controller operating at minimal losses. Figure 4.5 shows the input and out powers of the proposed controller against the cited benchmark control [14]. The difference between proposed and benchmark can be seen in the boom actuator input power. The proposed controller initially matches the benchmark at the start of motion but as the piston speed increases it switches to a minimum differential pressure mode which critically minimizes the power consumption. The power losses slightly increase at the end of the extension stroke as some throttling is introduced to match the reference force. However, the proposed controller outperforms even when throttling. During retraction both controllers exhibit similar performance as they both use an efficient differential mode.

Similar behavior is seen in the arm actuator, soon after the motion starts the proposed controller switches to a near minimum differential pressure mode reducing the power losses significantly. This can be observed during the acceleration phase of the extension stroke. Due to the reference force increasing the mode becomes infeasible and a compromise in power losses must be made, both controllers exhibit similar losses. As the piston retracts the proposed controller again chooses a highly efficient mode with minimal losses while the benchmark performance is poorer. Finally, both controllers show similar behavior during the rest of the retraction phase.

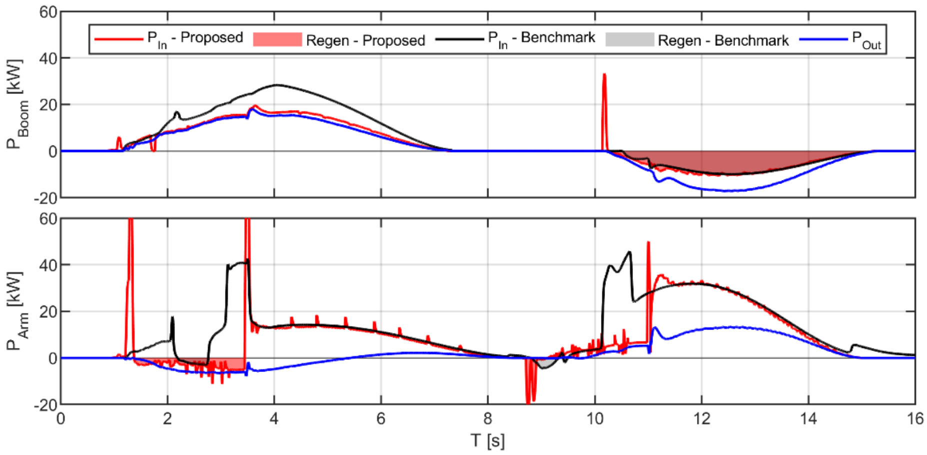

Figure 4.5: Power consumption of the proposed control algorithm against benchmark control

One key difference can be seen during the durations of pressure switching where the proposed controller concentrates the switch in a short time τ_{Sw} while the benchmark one takes longer contributing to higher losses. Another advantage of the proposed controller is that it can allow for slight negative force error which allows for more utilization of efficient modes. Although this reflects in the piston velocity where it decelerates and accelerates, the deviation is small and unnoticeable.

Figure 4.6 shows the input energy of the proposed control against the original machine's load sensing system and the benchmark control. The results demonstrate the effectiveness of the proposed MPS system and control algorithms in reducing power losses compared to the conventional load sensing (LS) system. The LS baseline exhibited total power consumption of 518 kJ. By introducing the MPS system with the benchmark controller, the losses were reduced to 250 kJ, corresponding to a 52% reduction. Further improvement was achieved with the proposed controller, where the energy consumption decreased to 176 kJ, representing a 67% reduction relative to the original LS system and an additional 32% reduction compared to the benchmark controller. These results highlight the significant efficiency gains enabled by the MPS architecture and the proposed control strategy.

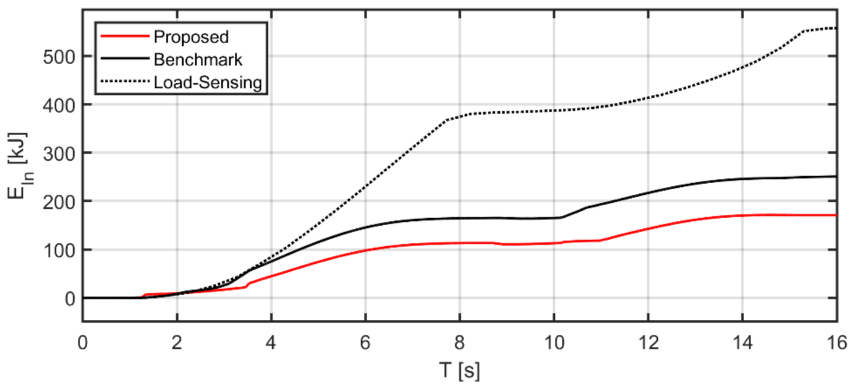

Figure 4.6: Input energy of proposed control algorithm against benchmark control

While these findings demonstrate the potential of the proposed control, it is important to note the limitations of the air grading cycle used for evaluation. The cycle does not fully represent real operating conditions. In particular, it may exaggerate the energy savings when compared to an LS system, which inherently shows higher compensation losses in no-load situations. Furthermore, the inclusion of energy recovery can distort the efficiency profile, suggesting greater savings than might actually occur under practical working conditions. Therefore, the results should be interpreted as an indication of relative system improvements rather than a direct prediction of real-world energy savings. The MPS along with the proposed controller are planned for future experimental work to provide more concrete energy saving estimates under real-world operating conditions.

5. Conclusion and Future work

This paper presented a novel control strategy for a Multi-Pressure System (MPS) for an excavator's work functions. Simulation results for boom and arm actuators demonstrated accurate tracking of position, velocity, and force references, while significantly reducing energy consumption. The proposed controller dynamically selects chamber pressures to minimize throttling losses and optimize efficiency. The proposed controller ability to operate at near-minimum pressure differential and tolerate slight force error allows for higher energy savings. The proposed method achieved up to 67% reduction in energy consumption compared to conventional Load Sensing (LS) systems and 32% compared to an MPS benchmark controller, highlighting its potential for improving the machine's overall efficiency.

6. References

[1] P. Achten, "Fundamentals of Hydraulic Transformers," in *14th International Fluid Power Conference*, Dresden, Germany: River Publishers, 2024, pp. 796–815. doi: 10.13052/rp-9788770042222C63.

[2] M. Linjama, H.-P. Vihtanen, A. Sipola, and M. Vilenius, "Secondary controlled multi-chamber hydraulic cylinder," in *The 11th Scandinavian International Conference on*

Fluid Power SICFP'09, Linköping, Sweden, June 2-4 2009, Linköping, Sweden, 2009. Accessed: June 07, 2024.

[3] J. Zimmerman, E. Busquets, and M. Ivantysynova, "40% Fuel Savings by Displacement Control Leads to Lower Working Temperatures - A Simulation Study and Measurements," in *Proceedings of the 52nd National Conference on Fluid Power*, Las Vegas, USA, Mar. 2011.

[4] Vukovic, "STEAM : a holistic approach to designing excavator systems," in *9th International Fluid Power Conference (9th IFK)*, 2014. Accessed: Mar. 19, 2024.

[5] D. Fassbender, C. Brach, and T. Minav, "Experimental Investigations of Partially Valve-, Partially Displacement-Controlled Electrified Telehandler Implements," *Actuators*, vol. 12, Jan. 2023, doi: 10.3390/act12020050.

[6] K. Heybroek and J. Sjöberg, "Model Predictive Control of a Hydraulic Multichamber Actuator: A Feasibility Study," *IEEE/ASME Transactions on Mechatronics*, vol. 23, no. 3, pp. 1393–1403, 2018, doi: 10.1109/TMECH.2018.2823695.

[7] R. Hansen, T. Andersen, and H. Pedersen, "Analysis of discrete pressure level systems for Wave Energy Converters," in *International Conference on Fluid Power and Mechatronics (FPM), 2011*, 2011, p. 558. doi: 10.1109/FPM.2011.6045825.

[8] M. Huova, M. Linjama, P. Kahra, J. Elonen, P. O. Box, and F. Oy, "New Implementation Of Digital Hydraulic Multi-Pressure Actuator," in *Workshop on Digital Fluid Power*, 2019.

[9] M. Huova and M. Linjama, "Energy efficient throttling control of a multi-pressure system using a genetic algorithm and model predictive control," *Proceedings of the Institution of Mechanical Engineers, Part I: Journal of Systems and Control Engineering*, vol. 236, no. 2, pp. 406–417, 2022, doi: 10.1177/09596518211027713.

[10] Z. Xu, M. Bertolin, A. Vacca, and J. Nilsson, "A Hydraulic Architecture Based on Multi-common Pressure Rail Principle Using Multi-chamber Cylinders for Excavators," in *Advancements in Fluid Power Technology: Sustainability, Electrification, and Digitalization*, L. Ericson and P. Krus, Eds., Cham: Springer Nature Switzerland, 2025, pp. 339–356. doi: 10.1007/978-3-031-84505-5_22.

[11] A. H. Hansen and H. C. Pedersen, "Reducing pressure oscillations in discrete fluid power systems," *Proceedings of the Institution of Mechanical Engineers, Part I: Journal of Systems and Control Engineering*, vol. 230, no. 10, pp. 1093–1105, Nov. 2016, doi: 10.1177/0959651815625015.

[12] M. Linjama and M. Huova, "Model-based force and position tracking control of a multi-pressure hydraulic cylinder," 2018, doi: 10.1177/0959651817754035.

[13] *JCMAS - Earthmoving machinery - Energy consumption test method - Hydraulic excavator*, 2010.

[14] M. Allam and M. Huova, "Energy Efficiency and Control of a Multi-pressure System - An Excavator Study," *International Journal of Fluid Power*.

Biographies

Mohamed Allam received a MSc degree at Ain Shams University, Egypt, in 2020. He is currently working as a doctoral researcher at Tampere University, Tampere Finland. He is pursuing a Ph.D. degree in Automation Science and Engineering. Mohamed is currently working in Tampere University's Innovative Hydraulics and Automation Lab. Mohamed's work is mainly in energy efficient machines, hybrid technologies, powertrains modelling and simulation.

Mikko Huova received a DSc degree at Tampere University of Technology, Finland, in 2015. The topic of his thesis is related to energy-efficient digital hydraulic systems, and he is continuing the work on this subject as a postdoctoral researcher at Tampere University. The areas of interest include energy efficient actuator systems, control design, modelling and simulation.

Kim Heybroek was born in Vastervik, Sweden, in 1981. He received the M.Sc. degree in mechanical engineering from Linkoping University (LiU), Linkoping, Sweden, in 2006. In 2008, he joined Volvo Construction Equipment in Eskilstuna, where he is currently working as a Research Engineer and has a specialist role in the field of hydraulics. In 2017, he received the Ph.D. degree in hydraulics at the Department of Fluid Power and Mechatronic Systems (FluMeS) at LiU.